Superconductivity at 44.4 K achieved by intercalating $EMIM^+$ into FeSe

Jinhua Wang(王晋花), Qing Li(李庆), Wei Xie(谢威), Guanyu Chen(陈冠宇), Xiyu Zhu(祝熙宇), and Hai-Hu Wen(闻海虎)

Citation: Chin. Phys. B, 2021, 30 (**10**): 107402. DOI: 10.1088/1674-1056/ac1f09
Journal homepage: http://cpb.iphy.ac.cn; http://iopscience.iop.org/cpb

What follows is a list of articles you may be interested in

Revealing the A_{1g}-type strain effect on superconductivity and nematicity in FeSe thin flake

Zhaohui Cheng(程朝晖), Bin Lei(雷彬), Xigang Luo(罗习刚), Jianjun Ying(应剑俊), Zhenyu Wang(王震宇), Tao Wu(吴涛), and Xianhui Chen(陈仙辉)

Chin. Phys. B, 2021, 30 (**9**): 097403. DOI: 10.1088/1674-1056/ac1efa

Doping effects of transition metals on the superconductivity of (Li,Fe)OHFeSe films

Dong Li(李栋), Peipei Shen(沈沛沛), Sheng Ma(马晟), Zhongxu Wei(魏忠旭), Jie Yuan(袁洁), Kui Jin(金魁), Li Yu(俞理), Fang Zhou(周放), Xiaoli Dong(董晓莉), and Zhongxian Zhao(赵忠贤)

Chin. Phys. B, 2021, 30 (**1**): 017402. DOI: 10.1088/1674-1056/abd2ab

Structural and electrical transport properties of Cu-doped $Fe_{1-x}Cu_xSe$ single crystals

He Li(李贺), Ming-Wei Ma(马明伟), Shao-Bo Liu(刘少博), Fang Zhou(周放), and Xiao-Li Dong(董晓莉)

Chin. Phys. B, 2020, 29 (**12**): 127404. DOI: 10.1088/1674-1056/abc3af

Anomalous spectral weight transfer in the nematic state of iron-selenide superconductor

C Cai(蔡淙), T T Han(韩婷婷), Z G Wang(王政国), L Chen(陈磊), Y D Wang(王宇迪), Z M Xin(信子鸣), M W Ma(马明伟), Yuan Li(李源), Y Zhang(张焱)

Chin. Phys. B, 2020, 29 (**7**): 077401. DOI: 10.1088/1674-1056/ab90ec

Electronic structure and spatial inhomogeneity of iron-based superconductor FeS

Chengwei Wang(王成玮), Meixiao Wang(王美晓), Juan Jiang(姜娟), Haifeng Yang(杨海峰), Lexian Yang(杨乐仙), Wujun Shi(史武军), Xiaofang Lai(赖晓芳), Sung-Kwan Mo, Alexei Barinov, Binghai Yan(颜丙海), Zhi Liu(刘志), Fuqiang Huang(黄富强), Jinfeng Jia(贾金峰), Zhongkai Liu(柳仲楷), Yulin Chen(陈宇林)

Chin. Phys. B, 2020, 29 (**4**): 047401. DOI: 10.1088/1674-1056/ab75d4

Superconductivity at 44.4 K achieved by intercalating EMIM$^+$ into FeSe*

Jinhua Wang(王晋花), Qing Li(李庆), Wei Xie(谢威), Guanyu Chen(陈冠宇), Xiyu Zhu(祝熙宇)†, and Hai-Hu Wen(闻海虎)‡

Center for Superconducting Physics and Materials, National Laboratory of Solid State Microstructures and Department of Physics, Collaborative Innovation Center of Advanced Microstructures, Nanjing University, Nanjing 210093, *China*

(Received 12 July 2021; revised manuscript received 11 August 2021; accepted manuscript online 19 August 2021)

Superconductivity with transition temperature T_c above 40 K was observed in protonated FeSe (H_y-FeSe) previously with the ionic liquid EMIM-BF_4 used in the electrochemical process. However, the real superconducting phase is not clear until now. And detailed structural, magnetization, and electrical transport measurements are lacking. By using similar protonating technique on FeSe single crystals, we obtain superconducting samples with T_c above 40 K. We show that the obtained superconducting phase is not H_y-FeSe but actually an organic-ion ($C_6H_{11}N_2^+$ referred to as EMIM$^+$)-intercalated phase (EMIM)$_x$FeSe. By using x-ray diffraction technique, two sets of index peaks corresponding to different c-axis lattice constants are detected in the obtained samples, which belong to the newly formed phase of intercalated (EMIM)$_x$FeSe and the residual FeSe, respectively. The superconductivity of (EMIM)$_x$FeSe with T_c of 44.4 K is confirmed by resistivity and magnetic susceptibility measurements. Temperature dependence of resistivity with different applied magnetic fields reveals that the upper critical field H_{c2} is quite high, while the irreversibility field H_{irr} is suppressed quickly with increasing temperature till about 20 K. This indicates that the resultant compound has a high anisotropy with a large spacing between the FeSe layers.

Keywords: FeSe, iron-based superconductor, electrochemical intercalation

PACS: 74.70.Xa, 74.25.–q, 74.72.Ek, 82.45.Aa **DOI:** 10.1088/1674-1056/ac1f09

1. Introduction

Iron-based superconductors have attracted vast interest in condensed matter physics and material science since it was discovered in 2008.[1] Among iron-based superconducting materials, the compound FeSe was reported to have the simplest structure with a critical transition temperature (T_c) of about 8 K at ambient pressure,[2] which is constituted by edge-sharing $FeSe_4$-tetrahedra layers stacking along the c-axis. By applying high pressures, a dome-shaped superconducting region with rich physics appears, and its T_c was enhanced up to 36.7 K at 8.9 GPa.[3,4] Due to the lack of charge carrier reservoir layers, it is natural to dope carriers into the FeSe planes by intercalation in order to increase its transition temperature. Intercalating guest elements or composites into adjacent FeSe layers is the most common way to achieve that goal.

In the beginning, the alkali metals were intercalated into FeSe by solid state reactions, through which $A_xFe_{2-y}Se_2$ (A = K, Rb, Cs, Tl, $x < 1$, $y < 1$) were synthesized with T_c around 32 K.[5–9] However, in order to satisfy the charge balance, phase separation occurs in the body of the material, leading to the coexistence of superconducting phase $A_xFe_{2-y}Se_2$ and antiferromagnetic insulating phase $A_2Fe_4Se_5$.[10–13] This prohibits a thorough and systematic investigation of the physical properties in those materials. Thus, it is necessary to have a low-temperature technique to prepare intercalated FeSe-layer materials. Due to the special character of dissolving multiple metals, liquid ammonia could help to insert not only alkali metals (Li, Na, K, etc.), but also alkali-earth metals (Ca, Sr, Ba) and rare-earth metals (Eu, Yb) into the FeSe bulk samples.[14–17] These metals are co-inserted with liquid ammonia molecules, thus the inserted molecules are closer to be neutral in charge comparing with the alkali metal ion with valence state of +1, the former causes relatively complete FeSe planes with a significant increase of the c-axis lattice constant. And the highest T_c of 46 K was reached among this series of superconductors.[14] Although a large increase of T_c was realized, the chemical activity of intercalating composites between the adjacent FeSe layers made those materials extremely unstable in air. Using the hydrothermal technique and improved hydrothermal ion-exchange process,[18–20] a stable compound $Li_{1-x}Fe_xOHFeSe$ with an ordered guest-layer $Li_{1-x}Fe_xOH$ was prepared with T_c up to 42 K.[20] Besides the inorganic molecules which are co-inserted with metals, organic molecules could also be intercalated into FeSe,[21–28] producing a series of superconductors with different c-axis lattice parameters. Due to the varying size of organic molecules, such as C_5H_5N, $(H_2N)C_nH_{2n}(NH_2)$, and $C_nH_{2n+3}N$ (n = 6, 8, 18),[21,24,28] the interlayer spacing could be largely stretched

*Project supported by the National Natural Science Foundation of China (Grant Nos. 12061131001 and 52072170) and the Strategic Priority Research Program of Chinese Academy of Sciences (Grant No. XDB25000000).

†Corresponding author. E-mail: zhuxiyu@nju.edu.cn

‡Corresponding author. E-mail: hhwen@nju.edu.cn

to a certain degree, and the largest c-axis lattice parameter of 55.7 Å was achieved in $Li_x(ODA)_yFe_{1-z}Se$ with T_c of about 42 K.[28]

Besides plenty of researches about alkali metals co-inserted with inorganic or organic molecules into FeSe, some new superconductors were also discovered simply by intercalating organic composites, forming for example $(C_2H_8N_2)_xFeSe$.[29] This may pave a new way to synthesize intercalated FeSe derivative superconductors. The intercalation of $C_2H_8N_2$ in FeSe made c-axis lattice parameter expanded up to 21.700(6) Å. Moreover, two other different organic ions, cetyltrimethyl ammonium (CTA^+) and tetrabutyl ammonium (TBA^+),[30,31] were successfully inserted into FeSe through electrochemical intercalation. It has been found that these two kinds of organic-ions intergrown with FeSe formed a bulk superconductivity showing T_c of 45 K and 50 K, with c-axis lattice parameter expanded up to 14.5 Å and 15.5 Å, respectively. Through the similar method, a new derivative of FeSe, the so called protonated FeSe (H_y-FeSe), was discovered with T_c of 41 K,[32] in which the existence of hydrogen was indicated by nuclear magnetic resonance (NMR) measurements. But it is unclear what is the real superconducting phase, and studies on the detailed structure and physical properties are lacking up to now.

In this work, we give detailed investigation on the above material, named as protonated FeSe, obtained through the same method and interactant, 1-ethyl-3-methylimidazolium tetrafluoroborate (EMIM-BF_4), as reported by Cui *et al.*[32] According to the x-ray diffraction (XRD) measurements, we show that the title compound has a highly expanded c-axis constant, thus we conclude that the relevant phase is not H_y-FeSe, but rather another organic-ion-intercalated FeSe [$(EMIM)_xFeSe$]. The T_c of this new FeSe-based superconductor is 44.4 K, as evidenced by the results of temperature dependent magnetic susceptibility and resistivity measurements. Note that our intercalated $(EMIM)_xFeSe$ samples are also not very stable in atmosphere, very similar to the $(TBA)_{0.3}FeSe$,[31] and after a few days it will degrade back to the pristine FeSe with T_c of about 8 K.

2. Experimental details

The schematic experimental setup of the electrochemical intercalation experiment is illustrated in Fig. 1(a).[32] As shown in the illustration, the positive and negative electrodes made of platinum are placed in an ionic-liquid container. Then this device is put into a heating mantle to maintain a certain temperature during the electrochemical process. The FeSe single crystal grown by means of chemical vapor transport technique is attached on the negatively charged electrode by silver paste,[33,34] while positive electrode Pt wire is placed right opposite to it. After loading the FeSe single crystal on the electrode, we add ionic liquid into the container till the sample is completely immersed. During the electrochemical process, a constant voltage of 4 V is applied and the temperature of the heating mantle is set to 355 K. After about three days of electrochemical reaction, the intercalated FeSe crystal is removed from the electrode and various measurements are taken after cleaning the silver paste and some residual reactants on the sample surface.

The XRD is conducted on a Bruker D8 Advanced diffractometer with the Cu K_α radiation at room temperature. The temperature dependent resistivity is measured by a physical property measurement system (PPMS-16 T, Quantum Design) through the typical four-probe method in different magnetic fields. The temperature dependent magnetic susceptibility is measured by Quantum Design PPMS with vibrating sample magnetometer (VSM), while the magnetic field is applied parallel to the c-axis of the sample.

3. Results and discussion

Figure 1(b) shows the XRD patterns of pristine FeSe single crystal and intercalated FeSe after the electrochemical reaction. No matter before or after the experiment, the sample remains having good crystallinity. Hence, the XRD patterns show an obvious c-axis orientation and all peaks are indexed perfectly as $(00l)$ on the basis of tetrahedral structure. The black solid line represents a series of $(00l)$ peaks of FeSe single crystal, which indicates a c-axis lattice parameter of 5.52 Å. Meanwhile, the red solid line contains two sets of peaks. One set of them shows the same diffraction peaks as the black line, belonging to the residual FeSe of the sample. The other set represents a new phase, which has a larger c-axis lattice parameter. The Miller indices $(00l)$ in Fig. 1(b) are assigned on the basis of a primitive tetragonal structure with the space group of $P4/nmm$, in which the c-axis lattice constant is 10.45 Å. While taking the space group of body-centered tetragonal $I4/mmm$, only even values of $h+k+l$ can appear in accordance with the extinction rule, and the c-axis lattice constant should be 20.88 Å. However, the precise symmetry needs more experiments to identify. Such an obvious increase of the c-axis lattice parameter suggests that some kind of molecules with big size has been inserted into the sample in the experiment and the spacing between adjacent FeSe layers is expanded. Considering the fact that the pristine FeSe is held on the negative electrode, we intend to conclude that the inserted molecules are most likely organic ions $EMIM^+$ from the ionic liquid. The schematic structure of this new phase is shown in Fig. 1(c). Considering the finite size for three dimensions of the organic ions, they probably arrange themselves with a specific orientation between the adjacent FeSe layers as shown in Fig. 1(c). However, this needs further verification by determining the internal structure.

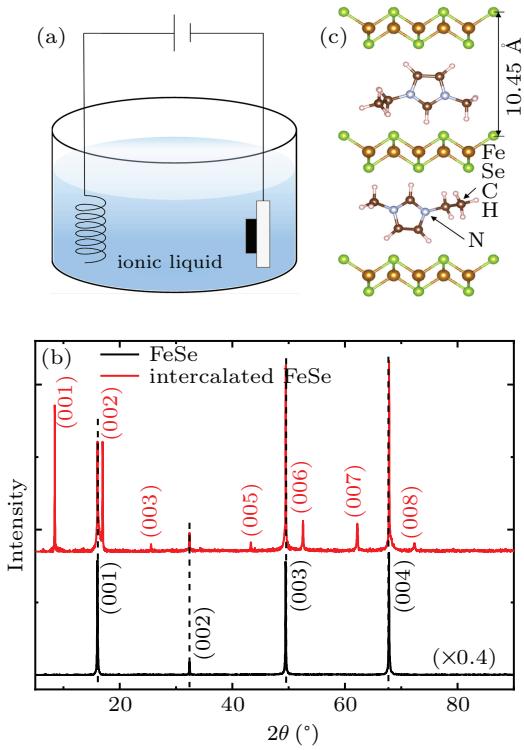

Fig. 1. (a) An illustration of the device for the electrochemical reaction. (b) XRD patterns of FeSe single crystal and intercalated FeSe. The Miller indices of the intercalated phase are colored by red, and those of FeSe phase are colored by black. (c) The schematic crystal structure of $(EMIM)_x$FeSe.

The temperature dependences of magnetic susceptibility and resistivity have been measured, and the results are shown in Fig. 2. It is worth mentioning that two samples from the same batch were used for the magnetic and transport measurements since the quality of the samples degraded quickly in the transfer process between two types of measurements. Figure 2(a) exhibits the temperature dependent magnetic susceptibility (χ–T curve) of intercalated FeSe, which is measured in zero-field-cooled (ZFC) and field-cooled (FC) modes with an applied magnetic field of 3 mT. The magnetic screening volume calculated from the ZFC data is about 437% comparable to the value reported previously in the similar systems,[30–32] which is larger than 100% as the demagnetization effect has not been taken into account. A sharp transition shows up at about 40 K in the χ–T curve, demonstrating the emergence of superconductivity. Note that the T_c of FeSe is around 8 K,[2] but this superconducting transition is not visible in the χ–T curve. The contradiction between XRD patterns and χ–T curve may be explained in the following way. One possible reason for the appearance of two phases in the XRD patterns is that the freshly intercalated sample is extremely unstable and some part of the sample with high T_c has degraded into the FeSe phase. It is found that, after exposing samples in air for some time, the content of the phase with high T_c superconductivity reduces and finally disappears, as revealed by XRD patterns and magnetizations, at the meantime the component of the FeSe phase increases. The time needed for preparing the magnetization and XRD measurements is different. In measuring the magnetization, the sample is quickly put into the sample chamber and cooled down, thus more and even complete content of the high T_c phase is sustained. However, the XRD measurements are conducted under ambient environment, usually for hours, during this process the sample which is supposed to be mainly composed by the high T_c phase will degraded, and some part will become FeSe. Thus, it is easy to understand the absence of the magnetization drop at about 8 K for FeSe for the freshly intercalated sample, but there are always two phases showing up in the XRD patterns. In order to check this scenario, we have measured temperature dependence of magnetization for samples with different durations after exposing to air. The results are shown in Fig. 5. Here we show the magnetization of a freshly intercalated sample with mainly the high T_c phase, and that after a long time exposing in air. One can see a clear evolution of the high T_c phase to FeSe. Thus for investigating the properties of the high T_c phase, the magnetization measurement must be done quickly after the intercalated samples are obtained. Figure 2(b) presents the temperature dependent resistivity under zero magnetic field with a current of 100 μA. There is a dramatic decrease of resistivity at 44.4 K, which is roughly consistent with the T_c obtained from the χ–T curve. The resistivity reaches zero at 38.5 K.

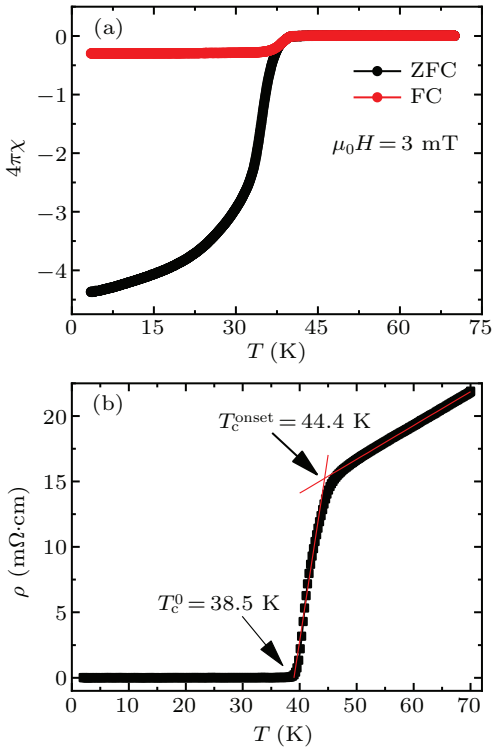

Fig. 2. (a) Temperature dependent magnetic susceptibility of intercalated FeSe single crystal measured in ZFC and FC modes under a magnetic field of 3 mT. (b) Temperature dependent resistivity under zero magnetic field.

In order to check the magnetic characteristics of the intercalated crystals, we have measured the temperature dependent magnetic susceptibility of intercalated FeSe in ZFC and

FC modes at different fields (M–T curves), and the results are shown in Fig. 3(a). At low fields, the ZFC curves show a trend of saturation. With increasing external magnetic fields, the magnetization value of the ZFC curve at low temperature is suppressed, which corresponds to the decrease of the magnetic screening volume. The inset of Fig. 3(a) shows the enlarged view of M–T curves near the transition. The deviation point of the ZFC and FC curves can be defined as the irreversible temperature $T_{\rm irr}$ in the external fields, and the $T_{\rm irr}$ decreases quickly with increasing applied magnetic field. The temperature dependence of irreversibility field $H_{\rm irr}(T)$ (M–T) of intercalated FeSe is shown in Fig. 4(b). Figure 3(b) shows the magnetization hysteresis loops (MHLs) at 3.5 K and 10 K, respectively. The MHLs show a typical magnetic hysteresis behavior of type-II superconductors. The width of MHL measured at 3.5 K is much wider than that at 10 K, and the ΔM of MHLs at low temperatures are comparable to those of other iron-based superconductors, like $(Li_{1-x}Fe_x)$OHFeSe,[35] which indicates the good vortex pinning of our samples.

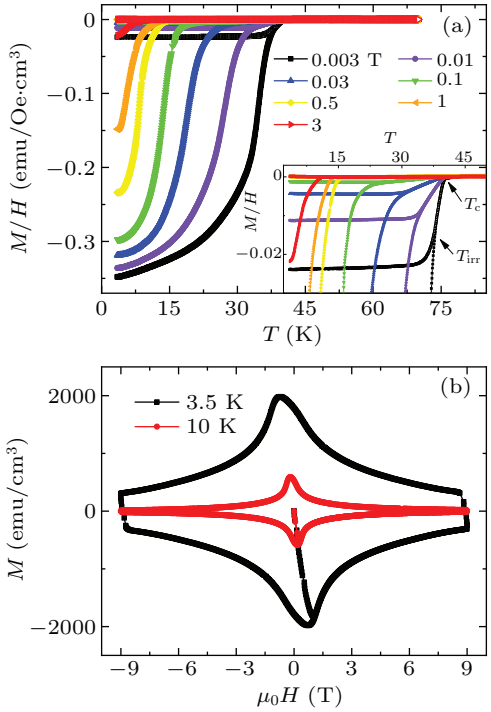

Fig. 3. (a) Temperature dependent magnetic susceptibility of intercalated FeSe single crystal measured at different magnetic fields. Inset shows the enlarged view of the M–T curves near the transition. (b) Magnetization hysteresis loops (MHLs) of intercalated FeSe single crystal at 3.5 K and 10 K.

Figure 4(a) displays the temperature dependent resistivity of another intercalated FeSe sample under different applied magnetic fields with a standard four-probe method. As we can see, the onset transition temperature $T_{\rm c}$ of intercalated FeSe is rather stable under external magnetic fields. In contrast to this, the zero-resistance temperature $T_{\rm c}$ decreases very fast with increasing magnetic fields, which is analogous to the situation of the M–T curves. Figure 4(b) gives the H–T phase diagram of the intercalated FeSe. The upper critical field $H_{\rm c2}$ and the irreversibility field $H_{\rm irr}$ as a function of temperature are obtained from the resistivity and magnetic susceptibility data. The $H_{\rm c2}$ is obtained by using the criterion of $95\%\rho_{\rm n}(T)$ in ρ–T curves, and the $H_{\rm irr}(\rho - T)$ is determined by using the criterion of $0.2\%\rho_{\rm n}(T)$, respectively. It can be seen that the $H_{\rm c2}$ shows a rather steep increase with lowering temperature, indicating a quite high upper critical field at zero temperature. The temperature dependence of $\mu H_{\rm c2}(T)$ exhibits an almost linear behavior near $T_{\rm c}$, which gives rise to a slope of $\mathrm{d}\mu_0 H_{\rm c2}/\mathrm{d}T = -2.17$ T/K. Thus the upper critical field at zero temperature calculated by the Werthamer–Helfand–Hohenberg (WHH) formula $\mu_0 H_{\rm c2}(0) = 0.69 T_{\rm c} |\mathrm{d}\mu_0 H_{\rm c2}/\mathrm{d}T|_{T_{\rm c}}$ is about 66.48 T.[36] According to the Ginzburg–Landau theory and Pippard formula, it is known that $\mu_0 H_{\rm c2} \approx \left(\pi\Phi_0/2\hbar^2\right)(\Delta/\upsilon_{\rm F})^2$ with Φ_0 the flux quanta, Δ the superconducting gap, and $\upsilon_{\rm F}$ the Fermi velocity. Thus, high value of $H_{\rm c2}(0)$ reflects a strong pairing gap. On the contrary, the irreversibility field $H_{\rm irr}$ decreases quickly with increasing temperature till about 20 K. Above 20 K, the $H_{\rm irr}$ drops slowly, leading to a wide region between the $H_{\rm irr}(T)$ and $H_{\rm c2}(T)$. It is known that above $H_{\rm irr}(T)$ there is finite dissipation, thus a wider region of vortex liquid is observed comparing with the original FeSe.[37] This broadening of superconducting transition is similar to other two-dimensional superconductors, such as $Li_{1-x}Fe_x$OHFeSe,[35] which suggests a large spatial distance between FeSe layers and a quite high anisotropy of intercalated FeSe samples. And then the $H_{\rm irr}(\rho - T)$ is fitted by the melting line of flux line lattice (FLL)[38]

$$\frac{t}{(1-t)^{1/2}}\frac{b^{1/2}}{1-b}\left(\frac{4(\sqrt{2}-1)}{(1-b)^{1/2}}+1\right)=\alpha, \qquad (1)$$

with $t = T/T_{\rm c}$, $b = H/H_{\rm c2}$, which is deduced from the Lindermann criterion.[39] The parameter α is given by the formula $\alpha = 2\pi(\varepsilon M_Z/M)^{-1/2}c^2$, with the Lindermann number $c \approx 0.15$–0.25 and $\varepsilon = 16\pi^3\kappa^4(k_{\rm B}T_{\rm c})^2/\Phi_0^3 H_{\rm c2}^0$, in which κ is the Ginzburg–Landau parameter. The mass ratio $(M_Z/M)^{1/2}$ becomes larger as the spacing distance between FeSe layers increases, where M_Z is a quasiparticle effective mass along the c axis and M describes the mass in the FeSe planes. The optimal result of $\alpha = 0.33$ is obtained by fitting $H_{\rm irr}(T)$ data. In the fitting process, the parameter κ in high-$T_{\rm c}$ superconductors usually takes a large value like $\kappa = 100$, such as when it equals to 95, the $H_{\rm irr}(T)$ data of $Bi_{2.2}Sr_2Ca_{0.8}Cu_2O_8$ could be well fitted by the melting criterion.[38] Thus, we take a general value of $\kappa = 100$ as the intercalated FeSe is a high-$T_{\rm c}$ superconductor ($T_{\rm c} = 44.4$ K). By substituting the $H_{\rm c2}(0)$, $T_{\rm c}$, and $c = 0.2$ into the formula of α, we get the mass ratio $(M_Z/M)^{1/2} \approx 44.5$, which is comparable with the value of a quasi-two-dimensional (quasi-2D) superconductor $Bi_{2.2}Sr_2Ca_{0.8}Cu_2O_8$ $[(M_Z/M)^{1/2} = 60]$,[38] and much larger

than that of 1.82 in FeSe,[37] 11 in $(Li_{1-x}Fe_x)$OHFeSe single crystal,[40] further proving the high spatial anisotropy of the sample.

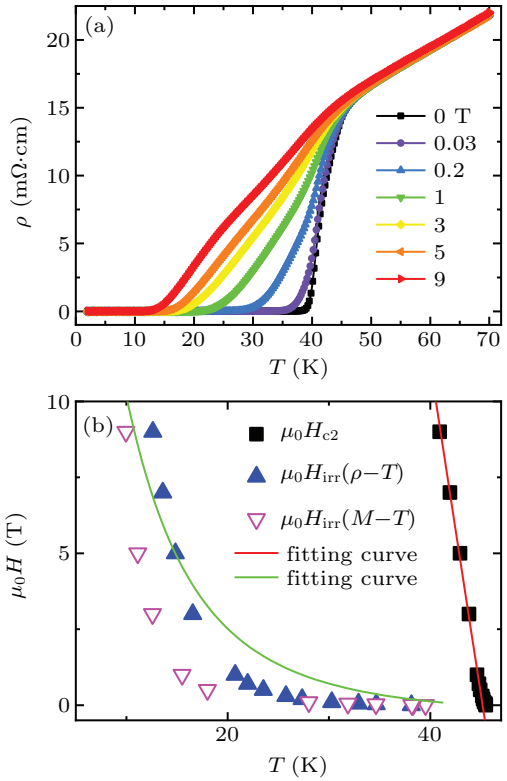

Fig. 4. (a) Temperature dependent resistivity under different applied magnetic fields. (b) H–T phase diagram of the intercalated FeSe. Black squares represent the upper critical field $H_{c2}(T)$ data. Blue (magenta) symbols represent the irreversibility field $H_{irr}(T)$ obtained from the temperature dependent resistivity (magnetic susceptibility) data. The red and green solid lines show the fitting results of $H_{c2}(T)$ and $H_{irr}(T)$, respectively.

Figure 5 shows the degradation situation of the intercalated FeSe sample. The magnetization measurements are conducted at a freshly intercalated sample mainly composed by the high T_c phase, and the same one after a long time exposing in air as shown in Fig. 5(a). The black squares show the results of magnetization measurement for the intercalated sample. One can clearly see a sharp superconducting transition at about 40 K, which is associated to the intercalated phase. At the meantime, the ZFC curve also drops a little at 8 K, which might be caused by the partial degradation of the sample. After exposing the sample in air for a long time, only the transition at 8 K is seen, which corresponds to the superconducting transition of FeSe, suggesting that the intercalated phase has degraded back to FeSe. Meanwhile, we also measure the XRD patterns after the magnetization measurements. As shown in Fig. 5(b), the XRD patterns of the freshly intercalated sample indicate that there are two phases with different c-axis lattice parameters. However only FeSe phase remains after a long time exposing the sample in air. The simultaneous disappearance of the high-T_c superconducting phase and the XRD patterns with larger lattice parameter further proves that the high T_c of the freshly intercalated sample is attributed to the intercalation of organic cations.

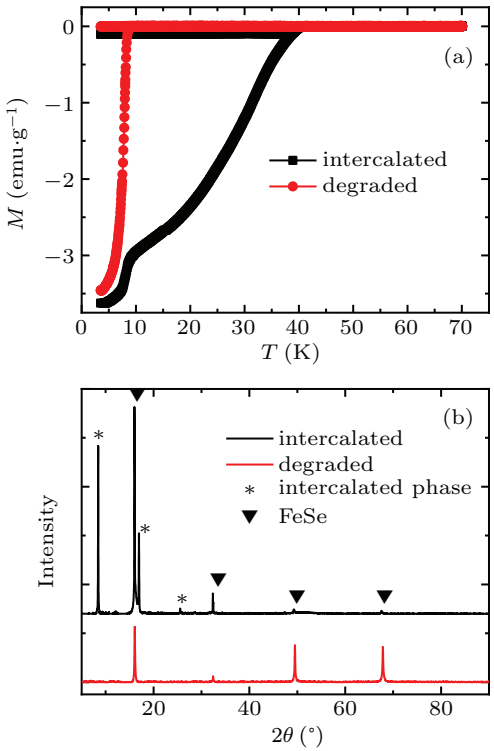

Fig. 5. (a) Temperature dependent magnetic susceptibility of a freshly intercalated sample and the one after degradation, which is measured in ZFC and FC modes with an applied magnetic field of 1 mT. (b) XRD patterns of the freshly intercalated and degraded phases. The peaks marked by star belong to the intercalated phase, and the rest marked by down-triangle belong to the FeSe phase.

4. Conclusions

We report superconductivity with transition temperature T_c above 40 K by electrochemically reacting FeSe with the ionic liquid of EMIM-BF_4. This phenomenon was recently reported as a process of protonating the FeSe crystals, but it was not clear what is the real superconducting phase. By doing x-ray diffraction measurements, we find a new set of diffraction peaks arising from the intercalated samples, these newly emergent peaks coexist with those of residual FeSe. We conclude that the newly emergent superconducting phase is the organic-cation ($C_6H_{11}N_2^+$, $EMIM^+$)-intercalated FeSe phase, namely, $(EMIM)_x$FeSe. Our results rule out the possibility that the high temperature superconducting phase is the simple protonated one H_y-FeSe. We also find that the upper critical field H_{c2} is quite high, indicating a strong pairing potential. While the irreversibility field H_{irr} is suppressed quickly with increasing temperature, showing a large region of vortex liquid in the phase diagram. By fitting the irreversibility line to the vortex melting formula deduced from the Lindermann criterion, we get a quite large mass ratio $(M_Z/M)^{1/2} \approx 44.5$, which is much larger than the value of FeSe and $(Li_{1-x}Fe_x)$OHFeSe single crystal. This also supports that the resultant material should

be highly anisotropic, as expected for a system with a large spacing between the FeSe layers.

Acknowledgment

We appreciate the kind help from Weiqiang Yu and Tianfeng Duan for establishing the device for the electrochemical reaction.

References

[1] Kamihara Y, Watanabe T, Hirano M and Hosono H 2008 *J. Am .Chem. Soc.* **130** 3296
[2] Hsu F C, Luo J Y, Yeh K W, Chen T K, Huang T W, Wu P M, Lee Y C, Huang Y L, Chu Y Y, Yan D C and Wu M K 2008 *Proc. Natl. Acad. Sci. USA* **105** 14262
[3] Medvedev S, McQueen T M, Troyan I A, Palasyuk T, Eremets M I, Cava R J, Naghavi S, Casper F, Ksenofontov V, Wortmann G and Felser C 2009 *Nat. Mater.* **8** 630
[4] Sun J P, Matsuura K, Ye G Z, Mizukami Y, Shimozawa M, Matsubayashi K, Yamashita M, Watashige T, Kasahara S, Matsuda Y, Yan J Q, Sales B C, Uwatoko Y, Cheng J G and Shibauchi T 2016 *Nat. Commun.* **7** 12146
[5] Guo J G, Jin S F, Wang G, Wang S C, Zhu K X, Zhou T T, He M and Chen X L 2010 *Phys. Rev. B* **82** 180520
[6] Krzton-Maziopa A, Shermadini Z, Pomjakushina E, Pomjakushin V, Bendele M, Amato A, Khasanov R, Luetkens H and Conder K 2011 *J. Phys.: Condens. Matter* **23** 052203
[7] Ying J J, Wang X F, Luo X G, Wang A F, Zhang M, Yan Y J, Xiang Z J, Liu R H, Cheng P, Ye G J and Chen X H 2011 *Phys. Rev. B* **83** 212502
[8] Wang A F, Ying J J, Yan Y J, Liu R H, Luo X G, Li Z Y, Wang X F, Zhang M, Ye G J, Cheng P, Xiang Z J and Chen X H 2011 *Phys. Rev. B* **83** 060512
[9] Fang M H, Wang H D, Dong C H, Li Z J, Feng C M, Chen J and Yuan H Q 2011 *EPL* **94** 27009
[10] Ye F, Chi S, Bao W, Wang X F, Ying J J, Chen X H, Wang H D, Dong C H and Fang M H 2011 *Phys. Rev. Lett.* **107** 137003
[11] Wang Z, Song Y J, Shi H L, Wang Z W, Chen Z, Tian H F, Chen G F, Guo J G, Yang H X and Li J Q 2011 *Phys. Rev. B* **83** 140505
[12] Ding X X, Fang D L, Wang Z Y, Yang H, Liu J Z, Deng Q, Ma G B, Meng C, Hu Y H and Wen H H 2013 *Nat. Commun.* **4** 1897
[13] Li W, Ding H, Deng P, Chang K, Song C L, He K, Wang L L, Ma X C, Hu J P, Chen X and Xue Q K 2012 *Nat. Phys.* **8** 126
[14] Ying T P, Chen X L, Wang G, Jin S F, Zhou T T, Lai X F, Zhang H and Wang W Y 2012 *Sci. Rep.* **2** 426
[15] Scheidt E W, Hathwar V R, Schmitz D, Dunbar A, Scherer W, Mayr F, Tsurkan V, Deisenhofer J and Loidl A 2012 *Eur. Phys. J. B* **85** 279
[16] Burrard-Lucas M, Free D G, Sedlmaier S J, Wright J D, Cassidy S J, Hara Y, Corkett A J, Lancaster T, Baker P J, Blundell S J and Clarke S J 2013 *Nat. Mater.* **12** 15
[17] Ying T P, Chen X L, Wang G, Jin S F, Lai X F, Zhou T T, Zhang H, Shen S J and Wang W Y 2013 *J. Am. Chem. Soc.* **135** 2951
[18] Lu X F, Wang N Z, Zhang G H, Luo X G, Ma Z M, Lei B, Huang F Q and Chen X H 2014 *Phys. Rev. B* **89** 020507
[19] Lu X F, Wang N Z, Wu H, Wu Y P, Zhao D, Zeng X Z, Luo X G, Wu T, Bao W, Zhang G H, Huang F Q, Huang Q Z and Chen X H 2015 *Nat. Mater.* **14** 325
[20] Dong X L, Jin K, Yuan D N, Zhou H X, Yuan J, Huang Y L, Hua W, Sun J L, Zheng P, Hu W, Mao Y Y, Ma M W, Zhang G M, Zhou F and Zhao Z X 2015 *Phys. Rev. B* **92** 064515
[21] Krzton-Maziopa A, Pomjakushina E V, Pomjakushin V Y, Rohr F V, Schilling A and Conder K 2012 *J. Phys. Condens. Matter* **24** 382202
[22] Hosono S, Noji T, Hatakeda T, Kawamata T, Kato M and Koike Y 2014 *J. Phys. Soc. Jpn.* **83** 113704
[23] Noji T, Hatakeda T, Hosono S, Kawamata T, Kato M and Koike Y 2014 *Physica C* **504** 8
[24] Hayashi F, Lei H, Guo J G and Hosono H 2015 *Inorg. Chem.* **54** 3346
[25] Hatakeda T, Noji T, Sato K, Kawamata T, Kato M and Koike Y 2016 *J. Phys. Soc. Jpn.* **85** 103702
[26] Miao X, Terao T, Yang X F, Nishiyama S, Miyazaki T, Goto H, Iwasa Y and Kubozono Y 2017 *Phys. Rev. B* **96** 014502
[27] Jin S F, Fan X, Wu X Z, Sun R J, Wu H, Huang Q Z, Shi C L, Xi X K, Li Z L and Chen X L 2017 *Chem. Comm.* **53** 9729
[28] Sakamoto C, Noji T, Sato K, Kawamata T and Kato M 2020 *J. Phys. Soc. Jpn.* **89** 115002
[29] Gao Z, Zeng S Y, Zhu B C, Li B, Hao Q Y, Hu Y W, Wang D K and Tang K B 2018 *Sci. China Mater.* **61** 977
[30] Shi M Z, Wang N Z, Lei B, Shang C, Meng F B, Ma L K, Zhang F X, Kuang D Z and Chen X H 2018 *Phys. Rev. Mater.* **2** 074801
[31] Shi M Z, Wang N Z, Lei B, Ying J J, Zhu C S, Sun Z L, Cui J H, Meng F B, Shang C, Ma L K ang Chen X H 2018 *New J. Phys.* **20** 123007
[32] Cui Y, Hu Z, Zhang J S, Ma W L, Ma M W, Ma Z, Wang C, Yan J Q, Sun J P, Cheng J G, Jia S, Li Y, Wen J S, Lei H C, Yu P, Ji W and Yu W Q 2019 *Chin. Phys. Lett.* **36** 077401
[33] Böhmer A E, Hardy F, Eilers F, Ernst D, Adelmann P, Schweiss P, Wolf T and Meingast C 2013 *Phys. Rev. B* **87** 180505
[34] Chen G Y, Wang E Y, Zhu X Y and Wen H H 2019 *Phys. Rev. B* **99** 054517
[35] Lin H, Xing J, Zhu X Y, Yang H and Wen H H 2016 *Sci. China-Phys. Mech. Astron.* **59** 657404
[36] Werthamer R, Helfand E and Hohenberg P C 1966 *Phys. Rev.* **147** 295
[37] Yang H, Chen G Y, Zhu X Y, Xing J and Wen H H 2017 *Phys. Rev. B* **96** 064501
[38] Houghton A, Pelcovits R A and Sudbø A 1989 *Phys. Rev. B* **40** 6763
[39] Lindermann F 1910 *Phys. Z* **11** 609
[40] Wang C L, Yi X L, Qiu Y, Tang Q B, Zhang X W, Luo Y S and Yu B H 2016 *Supercond. Sci. Technol.* **29** 055003